Reconsideration of the Rate Constant for the Reaction of Hydroxyl Radicals with Nitric Acid

Steven S. Brown,[†] Ranajit K. Talukdar,[‡] and A. R. Ravishankara*[,‡,§]

National Oceanic and Atmospheric Administration, Aeronomy Laboratory, R/E/AL2, 325 Broadway, Boulder, Colorado 80303

Received: December 11, 1998; In Final Form: February 22, 1999

We report rate coefficients for the reaction of OH with HNO_3, k_1, between 10 and 500 Torr of He, SF_6, N_2, and O_2 and at 10 different temperatures between 200 and 375 K. We generated OH via pulsed photolysis of HNO_3 and monitored the [OH] temporal profile via pulsed laser induced fluorescence. Below 300 K the value of k_1 increases rapidly with decreasing temperature and depends on pressure. The pressure dependence of k_1 at low temperature is significantly larger than that obtained by extrapolation of the currently available data. The pressure and temperature dependence is most likely due to a competition between direct abstraction and reactive complex formation. A rate constant expression derived from such a mechanism gives a global fit for k_1 that is applicable to atmospheric conditions. The new rate constant alters the calculated NO_2 to HNO_3 ratio in the lower stratosphere.

Introduction

Although the reaction of hydroxyl radicals with nitric acid plays an important role in NO_x (defined as the sum of NO and NO_2) chemistry in the upper atmosphere, there is still significant uncertainty in its rate constant and products at low temperature.[1]

$$OH + HNO_3 \rightarrow H_2O + NO_3 \quad (1a)$$

$$\rightarrow H_2O_2 + NO_2 \quad (1b)$$

Reaction 1a is the dominant product channel,[2] although some contribution from (1b) cannot be ruled out, as discussed further below. In addition to its atmospheric importance, reaction 1 is of fundamental interest because of its mechanism. The rate constant has been reported to display a strong negative temperature dependence and a weak but measurable pressure dependence below (but not above) room temperature.[1] These observations suggest a competition between direct abstraction of a hydrogen atom from nitric acid and association to form a reactive hydroxyl/nitric acid complex.

In the stratosphere, nitric acid serves as a reservoir for NO_x that is unreactive toward O_3. It is produced either by hydrolysis of N_2O_5 in the condensed phase or by the gas-phase association reaction of OH with NO_2.

$$OH + NO_2 + M \rightarrow HNO_3 + M \quad (2)$$

Destruction of nitric acid to regenerate NO_x occurs either by reaction 1 followed by photolysis of NO_3 or by direct photolysis.

$$HNO_3 + h\nu \rightarrow OH + NO_2 \quad (3)$$

Initial measurements of k_1 suggested that it was small ($<10^{-13}$ cm^3 $molecule^{-1}$ s^{-1}) and that it showed at most only a weak temperature dependence.[3,4] Because the reaction appeared to proceed via simple H atom abstraction, a pressure dependence was not expected, and the authors of the early studies did not examine this question. A later study by Wine et al.[2] using a flash photolysis−resonance fluorescence apparatus showed that k_1 was significantly larger than originally thought and that it displayed a strong negative temperature dependence. These authors pointed out the important implications of the larger k_1 values for model calculations of NO_x levels and ozone loss rates in the stratosphere. The significant impact of the larger rate constant led to a flurry of interest in reaction 1.[5−15] Most studies confirmed the larger rate constants and negative temperature dependence, although some discrepancies remained. Two studies[9,15] established that in addition to a negative temperature dependence, the reaction displayed a measurable pressure dependence at low temperature. Margitan and Watson[9] first demonstrated this effect over the pressure range 10−100 Torr in He, Ar, and SF_6 buffer gases. They found the room-temperature pressure dependence to lie within the error bars of a typical experiment, explaining why previous studies had overlooked it. Stachnik et al.[15] measured k_1 in 10, 60, and 730 Torr of He, N_2, and SF_6 at both room temperature and 248 K, confirming a clear pressure dependence. Their study provides the only currently available measurement of the variation of k_1 with pressure in N_2 buffer gas.

Because the rate constant for reaction 1 (k_1) strongly affects the balance between NO_x and HNO_3, and because there are no previous measurements of the pressure dependence in N_2 or O_2 buffer gases at temperatures below 250 K, we undertook a reexamination of k_1 over the pressure range 10−500 Torr in He, N_2, O_2, and SF_6 at temperatures between 200 and 375 K. We used pulsed laser photolysis to generate OH in excess HNO_3 and detected OH via laser-induced fluorescence (LIF). Our results agree well with most of the previous flash photolysis/OH fluorescence studies; however, because of more extensive measurements, we are able to show that k_1 is significantly larger at lower temperatures and higher pressures than the current

* Address correspondence to this author. E-mail: ravi@al.noaa.gov.
[†] NOAA NRC Postdoctoral Research Fellow.
[‡] Also affiliated with the Cooperative Institute for Research in the Environmental Sciences, University of Colorado, Boulder, CO 80309.
[§] Also affiliated with the Department of Chemistry, University of Colorado, Boulder, CO 80309.

10.1021/jp984721k CCC: $18.00
Published on Web 04/01/1999

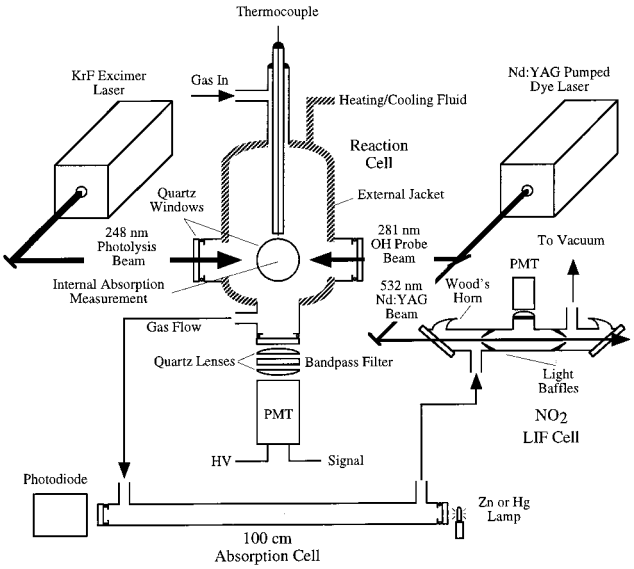

Figure 1. Experimental apparatus showing the pulsed photolysis laser induced fluorescence cell. Also pictured is the HNO_3 concentration measurement both inside the reaction cell and in an external absorption cell and the LIF measurement of the NO_2 impurity level. Because of strong quenching of NO_2* by buffer gases other than He, the NO_2 level was only measured at low (~10 Torr) He pressure prior to an experimental run in another gas or at higher pressures.

NASA/JPL recommendations for atmospheric modeling.[1] Fits to the new data show that the limiting high-pressure rate constant has a very strong negative temperature dependence. Current recommendations thus underestimate k_1 at temperatures and pressures characteristic of the lower stratosphere and upper troposphere.

Experimental Section

Fluorescence Cell and OH Detection. The experimental apparatus, shown in Figure 1, is similar to that used in previous kinetic studies in this laboratory.[16] This section briefly describes the general features of the apparatus, and the following two sections detail the modifications to the apparatus made to measure k_1.

The OH radicals were produced by 248-nm photolysis of a small fraction of the HNO_3 reactant with a KrF excimer laser. The initial OH concentration, as calculated from the measured photolysis laser fluence and the known 248-nm HNO_3 cross section,[17] was maintained at $[OH]_0 \leq 4 \times 10^{11}$ cm^{-3}. We adjusted the photolysis laser fluence by inserting different neutral density filters at each nitric acid concentration so that $[OH]_0$ did not vary with $[HNO_3]$ during the course of a rate constant measurement. A factor of 4 variation of $[OH]_0$ also did not affect the measured rate constants. We monitored the temporal profile of the OH concentration by LIF using the frequency-doubled output of a dye laser pumped by the 532-nm second harmonic of a Nd:YAG laser. The LIF laser excited the $Q_1(1)$ line of the off-diagonal A ($v' = 1$) ← X ($v'' = 0$) transition in OH at 281.91 nm (in air),[18] and a photomultiplier tube (PMT) collected OH diagonal fluorescence (either 1 → 1 or 0 → 0) through a 309 ± 6 nm (fwhm) band-pass filter that rejected scattered laser light at 282 nm. We scanned a portion of the OH LIF excitation spectrum including the $Q_1(1) \rightarrow Q_1(4)$ lines in order to verify that the excitation wavelength was correct, but we did not run kinetic experiments while monitoring rotational lines other than $Q_1(1)$. The Pyrex reaction cell had four quartz windows at right angles for introduction of the photolysis and the LIF laser beams, which crossed at right angles in most experiments, and a fifth window on the bottom for viewing OH fluorescence perpendicular to the plane of the laser beams. In some experiments, the photolysis and probe beams counterpropagated through the same set of windows, as shown in Figure 1.

The linear gas flow velocity through the 150 cm^3 reaction cell volume was 5−10 cm s^{-1} at all pressures, fast enough to refresh the gas mixture in the reaction zone every 1−2 laser shots in this 10 Hz experiment. Variation of the linear flow velocity had no effect on the measured rate constants. Anhydrous nitric acid was stored in a Pyrex bubbler, and the vapor was introduced into the reaction cell at concentrations between 6×10^{14} and 1.3×10^{16} cm^{-3} (see Table 1) using a small, variable flow of the bath gas. The nitric acid bubbler was mounted in a temperature controller immersed in a dry ice/ethanol bath. The temperature controller maintained a constant temperature between 234 and 273 K in order to regulate the vapor pressure of the liquid nitric acid. This procedure allowed easy control of the gas-phase nitric acid concentrations over a wide range of buffer gas pressures and flow rates. Methanol or ethylene glycol circulated through a jacket surrounding the reaction cell to control the reaction temperature. A thermocouple mounted just above the laser beams measured the gas temperature.

Nitric Acid Concentration Measurement. We measured gas-phase HNO_3 concentrations by absorbance of the 213.86-nm line from a Zn lamp in a room-temperature, 100-cm absorption cell located downstream from the reaction cell. The detector consisted of a photodiode and a band-pass filter centered at 214 nm with a fwhm of 22 nm. From the room-temperature absorption cross section of nitric acid of Burkholder et al.,[17] we interpolated a value of $\sigma = (4.52 \pm 0.19) \times 10^{-19}$ cm^2 at 213.86 nm. The 4.2% uncertainty (2σ) in this cross section arises from both the measured uncertainty in the cross section and the estimated uncertainty in the wavelength in the above study. We checked the stability of the Zn lamp by periodically measuring the zero in the absence of nitric acid. Over the course of any one rate constant measurement, the lamp intensity was stable to approximately 0.1%, and the measured uncertainty in the fits of the k' plots (described below) accounted for any small intensity fluctuations.

Two modifications to the concentration measurement were necessary at low temperature. First, the maximum usable nitric acid concentration was small at low temperatures because of the decrease in the vapor pressure. To measure the smaller concentrations, we used 184.9-nm light from an Hg lamp and a solar blind phototube on the external absorption cell when the reaction cell temperature was 200 K. The large HNO_3 cross section (1.63×10^{-17} cm^2 [17,19]) at this wavelength provided the necessary sensitivity.

Second, even at partial pressures well below its vapor pressure, nitric acid tended to adsorb on the Pyrex surfaces of the reaction cell at temperatures below its freezing point (231 K). Under these conditions it was necessary to ensure that the $[HNO_3]$ measured in the external absorption cell accurately reflected that present in the reaction cell. We therefore made an additional absorption measurement at 185 nm directly inside the reaction cell. In this configuration, the photolysis and LIF beams propagated along the same axis and the absorption was measured perpendicular to the laser beams (as in Figure 1). The path length across the reaction cell was 7.5 cm. We checked the temperature dependence of the HNO_3 cross section at 185 nm by measuring the relative absorption in a pair of 100-cm absorption cells, one at room temperature and the other at low temperature; the cross section varied by less than 2% with

TABLE 1: Measured OH + HNO_3 Rate Constants (in Units of 10^{-13} cm^3 $molecule^{-1}$ s^{-1})

		M = N_2		M = O_2		M = He		M = SF_6	
T (K)	[HNO_3] range (10^{15} cm^{-3})	P (Torr)	k_1	P (Torr)	k_1	P (Torr)	k_1	P (Torr)	k_1
200	0.06−0.4	19.8	6.51 ± 0.56						
		49.9	10.0 ± 1.1						
		100.2	11.2 ± 1.0						
		146.9	12.2 ± 2.1						
210	0.1−1.5	19.9	4.55 ± 0.71			20.9	3.76 ± 0.39		
		50.6	7.24 ± 1.24			50.3	4.39 ± 0.41		
		75.0	7.20 ± 0.58			99.8	5.85 ± 0.38		
		100.2	8.21 ± 0.93			199.9	7.27 ± 0.62		
		150.1	8.51 ± 0.96			499.0	8.55 ± 0.96		
		201.5	8.48 ± 1.22						
		299.8	9.68 ± 1.55						
		499.3	11.1 ± 3.0						
220	0.15−2.1	20.2	3.51 ± 0.30			19.6	2.74 ± 0.19		
		50.0	4.92 ± 0.36			50.2	3.52 ± 0.25		
		75.0	5.42 ± 0.38			100.5	4.51 ± 0.29		
		100.7	6.09 ± 0.42			200.6	5.42 ± 0.63		
		150.6	6.31 ± 0.37			497.5	6.74 ± 0.50		
		200.1	6.52 ± 0.46						
		302.1	6.94 ± 0.54						
		499.4	8.04 ± 0.64						
235	0.25−5.0	19.9	2.85 ± 0.14			10.1	2.31 ± 0.16	20.1	3.08 ± 0.16
		50.1	3.60 ± 0.19	49.4	3.50 ± 0.20	19.9	2.38 ± 0.17	99.6	4.24 ± 0.24
		100.0	4.07 ± 0.18			50.0	2.79 ± 0.16	500.2	5.43 ± 0.46
		198.8	4.69 ± 0.22			99.8	3.27 ± 0.16		
		498.7	5.05 ± 0.32			199.1	3.67 ± 0.21		
						498.9	4.27 ± 0.19		
250	0.5−10	20.0	2.30 ± 0.11			10.0	1.95 ± 0.13	20.0	2.37 ± 0.12
		50.0	2.60 ± 0.13			20.1	2.05 ± 0.12	99.8	2.87 ± 0.14
		100.2	2.80 ± 0.15			49.8	2.29 ± 0.14	498.8	3.25 ± 0.17
		200.6	2.94 ± 0.16			100.0	2.56 ± 0.13		
		500.8	3.07 ± 0.17			200.6	2.85 ± 0.18		
						500.1	3.08 ± 0.17		
273	0.5−12	19.6	1.57 ± 0.09	19.7	1.56 ± 0.10	20.0	1.54 ± 0.10	20.1	1.64 ± 0.09
		49.9	1.88 ± 0.10			49.8	1.67 ± 0.08	100.2	1.93 ± 0.09
		100.1	2.00 ± 0.10	99.5	2.05 ± 0.11	99.9	1.85 ± 0.08	498.2	2.15 ± 0.10
		199.9	2.01 ± 0.09			200.5	1.92 ± 0.09		
		498.6	2.05 ± 0.11			495.6	2.05 ± 0.09		
296	0.9−12	19.8	1.25 ± 0.07			20.2	1.21 ± 0.07	23.7	1.25 ± 0.06
		50.0	1.39 ± 0.06	50.0	1.37 ± 0.07	100.5	1.46 ± 0.07		
		100.2	1.47 ± 0.08			100.0	1.41 ± 0.06	498.0	1.62 ± 0.07
		199.5	1.51 ± 0.07			200.2	1.50 ± 0.07		
		499.6	1.54 ± 0.11			498.4	1.54 ± 0.07		
325	0.9−12	20.5	1.10 ± 0.06			20.4	1.13 ± 0.06	20.0	1.07 ± 0.05
		50.0	1.06 ± 0.06			50.0	1.16 ± 0.07	99.8	1.11 ± 0.05
		99.8	1.14 ± 0.06	99.8	1.18 ± 0.06	499.8	1.19 ± 0.06		
		200.0	1.14 ± 0.07			199.9	1.19 ± 0.05		
		498.6	1.16 ± 0.07			499.6	1.19 ± 0.05		
350	0.7−12	19.8	0.99 ± 0.07			20.1	1.04 ± 0.05	19.9	0.95 ± 0.05
		99.7	1.09 ± 0.06			50.0	1.07 ± 0.06	100.0	0.98 ± 0.05
		500.1	1.11 ± 0.07			99.5	1.03 ± 0.05	500.3	1.13 ± 0.06
						200.3	1.09 ± 0.06		
						500.7	1.05 ± 0.06		
373	0.9−13					99.8	1.02 ± 0.05		

temperature. Concentrations measured by absorption inside the reaction cell were the same as those measured in the external cell to within 5%. We used the external absorption measurement to calculate all rate constants reported here.

Determination of NO_2 Impurity Level. Because k_1 showed an unusual pressure and temperature dependence, it was important to establish that the observed behavior was not due to a contribution from the pressure dependent association reaction of OH radicals with the NO_2 impurity that was inevitably present in the HNO_3 sample. We measured the NO_2 concentration in the reaction mixture via 532-nm LIF in a second fluorescence cell located downstream from the external absorption cell (see Figure 1). A beam splitter separated approximately 20 mJ of the Nd:YAG second harmonic just prior to the dye laser. After collimation, the light propagated along the length of a 2.5-cm diameter cylindrical fluorescence cell that had Brewster angle windows, Wood's horns, and baffles to reduce scattered light. A red sensitive PMT viewed NO_2 fluorescence through *f*/*l* optics and a series of cutoff filters that rejected most of the scattered 532-nm laser light but passed NO_2 fluorescence at $\lambda > 600$ nm. The NO_2 fluorescence spectrum is broad and diffuse and extends several hundred nanometers to the red of the excitation wavelength.[20] Because the most important limitation to the detection sensitivity was quenching of NO_2 fluores-

cence, we measured the NO_2 content of the HNO_3 sample at low pressure in He. Under these conditions, HNO_3 was the most effective quencher. Therefore, we calibrated the NO_2 fluorescence intensity by adding known quantities of NO_2 to a flowing reaction mixture that included HNO_3 vapor. The NO_2 content of the HNO_3 vapor did not vary measurably over a range of 10−50 Torr of He buffer gas, and we do not expect it to change significantly at higher pressures or in different bath gases.

The measured fraction of NO_2 in HNO_3 was $(0.2-1.0) \times 10^{-4}$, low enough that the OH + NO_2 reaction is an insignificant contributor to measured OH loss rates. In some cases, photolysis of HNO_3 was a comparably large NO_2 source. We measured the NO_2 level at HNO_3 concentrations ranging from 5×10^{15} to 2×10^{16} and found no dependence on [HNO_3]. Other factors, including the age of the HNO_3 sample, the condition for storage, and the carrier gas flow rate through the liquid sample during use were important in the amount of NO_2 contamination. In particular, the NO_2 concentrations were quite high (10−100 times higher than the fractions listed above) upon first use of a sample that had been stored overnight. The NO_2 was removed as carrier gas flowed through the liquid HNO_3 reservoir, and approximately 10−20 min of carrier gas flow through the liquid HNO_3 reservoir brought the NO_2 fraction to a steady value within the range listed above. Therefore, we flowed the carrier gas through the bubbler for about a half hour prior to making rate constant measurements. Even at the highest measured NO_2 concentrations and lowest temperatures, reaction with NO_2 accounted for less than 1% of the total measured OH loss rate.

Other potential impurities in anhydrous HNO_3 samples include NO_3 and N_2O_5.[21] The NO_3 level in gas-phase HNO_3 is generally smaller than that of NO_2 and thus should have no influence on measured OH loss rates. We can rule out possible influence from N_2O_5 since its concentration depends strongly on the amount of water present in the HNO_3 sample. We measured k_1 under similar conditions of pressure and temperature using both anhydrous HNO_3 samples and using commercially available 70% HNO_3 (with the NO_2 distilled out as described above) and found the rate constants to be the same to within experimental uncertainty. Furthermore, we added small amounts of water to the anhydrous HNO_3 in order to suppress N_2O_5 formation. Thus, although we have not directly measured NO_3 or N_2O_5 impurity levels, we do not anticipate that they influence our measurements.

We synthesized anhydrous HNO_3 by adding concentrated sulfuric acid to solid sodium nitrate at low pressure and collecting the evolving nitric acid vapor in a liquid nitrogen cooled trap. We stored the sample in a freezer at 243 K in the dark and used it without further purification other than the daily distillation procedure described above.

Results

Figure 2 displays a typical set of OH temporal profiles in excess HNO_3 ([HNO_3] > 10^3 [OH]$_0$). The following equation represents the temporal profile of the OH concentration.

$$\ln\left(\frac{[OH]}{[OH]_0}\right) = -(k_1[HNO_3] + k_d)t = -k't \qquad (4)$$

Here k' is the observed first-order loss rate constant, and k_d is the first-order OH loss rate constant in the absence of HNO_3 (not directly measured) due to diffusion, reaction with impurities in the buffer gas, and flow out of the reaction zone. We typically observed an OH concentration change over 2−3 orders of magnitude and fit the observed decays to eq 4 to determine k'

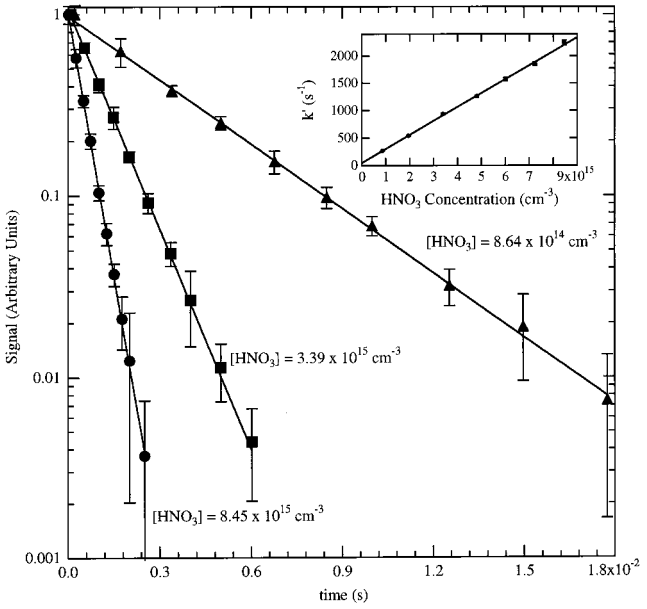

Figure 2. Typical set of OH temporal profiles (ln [OH] vs t) in excess nitric acid (P = 50 Torr of N_2, T = 250 K). The slope of the lines gives k', the pseudo-first-order rate constant, and the slope of a plot of k' vs nitric acid concentration, shown in the inset, gives the bimolecular rate constant, k_1.

with a precision of 2−5% (2σ). The slope of a plot of k' against the measured [HNO_3] gave k_1, as the inset in the figure shows. To obtain each bimolecular rate constant, we measured approximately seven pseudo-first-order rate constants spanning more than 1 order of magnitude in HNO_3 concentration. The intercepts (k_d) of the k' vs [HNO_3] plots varied between 20 and 100 s^{-1} depending on buffer gas, total pressure and temperature. The lack of curvature in the k' vs [HNO_3] plots shows that HNO_3 is not a highly more efficient collision partner than the bath gas and that we can neglect the collisional stabilization by HNO_3 to the measured pressure dependence in k_1.

Table 1 presents the measured k_1 as a function of temperature, pressure, and bath gas. The temperatures listed in the table are accurate to ±0.5 K, and the pressures to ±0.3 Torr. The uncertainties in the rate constants come from the 2σ precision of the k' plots and the uncertainties in the HNO_3 absorption cross sections. Because our primary interest was in defining k_1 under atmospheric conditions, the data set is more extensive for N_2 than for He or SF_6, particularly at low temperature. The data in He and SF_6 were useful in determining the approach to high- and low-pressure behavior of the k_1, as described in the next section. There are several additional k_1 measurements in O_2. Because O_2 is a very efficient OH fluorescence quencher, measurements of OH decays in O_2 were significantly more difficult and only a few values of k_1 in O_2 appear in Table 1. Our data show, however, that there is no difference between k_1 measured in N_2 and O_2 bath gases to within the experimental uncertainty. Figure 3 illustrates this point with a plot of k' vs [HNO_3] in O_2 and N_2 at two pressures at 273 K.

Discussion

A. Pressure Dependences. Figure 4 displays our measured values of k_1 in He and N_2 over the pressure range 10−500 Torr at 296, 250, and 220 K. The data from several other studies, including those from Stachnik et al.,[15] Margitan and Watson,[9] and Devolder et al.[12] also appear in the figure. The first two sets of literature data are compared because they are the only previous studies that explicitly considered a pressure dependence

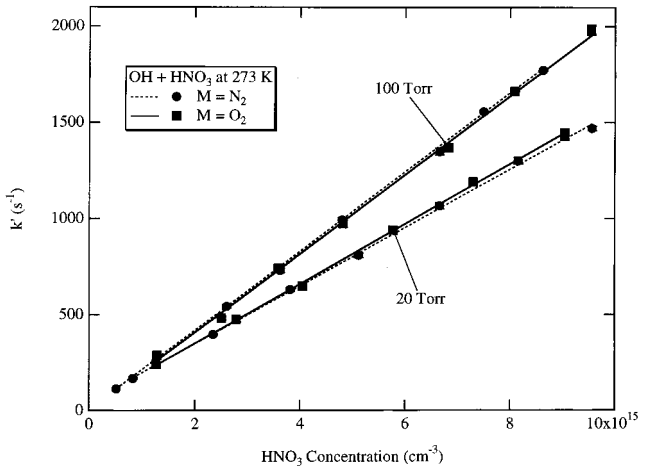

Figure 3. Plot of the pseudo-first-order rate constant for loss of OH vs nitric acid concentration in 20 and 100 Torr of O_2 and N_2 at 273 K. Linear fits to the data for each buffer gas give the same slope to within the experimental uncertainty.

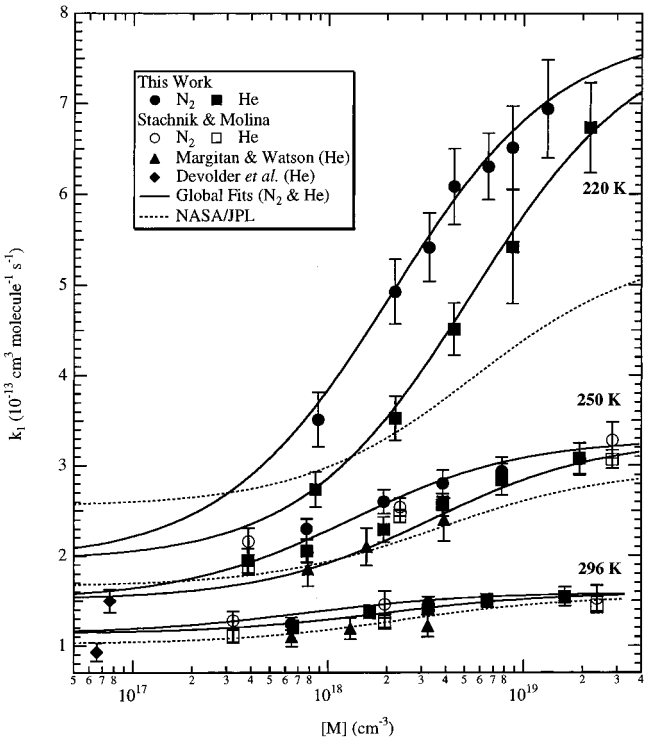

Figure 4. Pressure dependence of k_1 at 296, 250, and 220 K. The plots display data from this work for N_2 and He buffer gases as well as relevant literature data, as the legend shows. The solid lines are fits of our data plus several literature studies to eq 5 (see text). The upper solid curve at each temperature corresponds to N_2 buffer gas, and the lower, to He. The dashed line is the current NASA/JPL recommendation for the pressure dependence of k_1 at each temperature.

for this reaction. The third study is representative of the low pressure measurements. The low pressure data are consistent with the observed variation of k_1 at higher pressure, and they provide a useful estimate of the low-pressure limiting bimolecular rate constant. (In this paper, the low-pressure limiting rate constant is simply the value of k_1 at low pressure where it is independent of pressure rather than the conventional definition for an association or decomposition reaction.) Our results agree with previous studies, particularly with the data of Stachnik et al.,[15] the only previous investigators who examined the pressure dependence of k_1 in N_2, albeit by a few measurements (10, 60, and 730 Torr at both 297 and 248 K). The values of k_1 in He from Margitan and Watson[9] are somewhat smaller than our He measurements; however, the differences between the two measurements lie within the combined uncertainties. The solid lines in Figure 4 are global fits to all of the data. We discuss the form of the fitting function, its origin and the data included in the fit further below. The dashed lines are the current NASA recommendation[1] for k_1 for atmospheric modeling.

The pressure dependence at 296 K is weak but discernible. Our data show an approximately 25% increase in k_1 from 20 to 500 Torr, and no strong dependence on the identity of the buffer gas. Several previous studies found no pressure dependence for k_1,[13] probably in part because the effect is small at room temperature. The difference between rate constants at high and low pressures lies within the uncertainty of some experiments, and the effect due to the buffer gas identity is negligible. The NASA/JPL recommendation[1] for k_1 at 296 K is 5−10% smaller than our values over the entire pressure range, although the difference is close to the uncertainty in our data. The recommendation (for N_2/O_2) agrees well with k_1 measured in He by Margitan and Watson.[9]

The middle traces in Figure 4 show the somewhat stronger pressure dependence at 250 K. There is an approximately 2-fold change in k_1 from 20 to 500 Torr and a clear dependence on the identity of the buffer gas. Interestingly, however, Table 1 shows that although there is a large difference between values of k_1 in He and N_2, there is almost no difference between these values in N_2 and SF_6. The lack of difference between the latter two gases is unusual, but it has been seen in other studies,[2,15] and it may be another reason the pressure dependence of k_1 initially went unrecognized. The NASA/JPL recommendation[1] at 250 K falls approximately 20% below our N_2 rate constants over most of the pressure range. As in the room-temperature data, the recommendation appears to fit the He data of Margitan and Watson[9] but does not reproduce the k_1 values relevant to the atmosphere. The low-pressure rate constant of Devolder et al.[12] agrees well with the low-pressure limit of the global fits.

The 220 K data in the upper traces of Figure 4 show a 4-fold difference between the low- and high-pressure rate constants. There is relatively little literature data with which to compare at this temperature. Marinelli and Johnston[8] reported k_1 values at 218 K that fall at the low-pressure end of the fits in Figure 4 and agree, within their uncertainty, with our results. The 220 K NASA/JPL recommendation[1] underestimates the N_2 rate constants by 50% at the highest pressures measured.

We were unable to measure a pressure dependence above 300 K. There are fewer k_1 measurements in Table 1 above 300 K than below, in part because the lack of a pressure dependence requires fewer measurements to characterize the rate constant, and in part because the high-temperature rate constants have less relevance to the atmosphere.

The k_1 values in Table 1 agree well (i.e., to within the experimental uncertainty) with many of the previous studies of reaction 1 that did not consider a pressure dependence,[2,5,7,8,10] as long as we explicitly include the pressure at which the previous measurements were made. As such, the new measurements do not represent a departure from previous ones, but rather an expansion of the number of measurements and the range of pressures and temperatures. As noted in the Experimental Section, the usual tests for contributions from secondary reactions were negative. The careful measurement of the nitric acid vapor concentrations at low temperature and the measurement of the NO_2 impurity content serve to further increase the confidence in the rate constants reported here. Finally, we note that the values of k_1 measured with water vapor absent

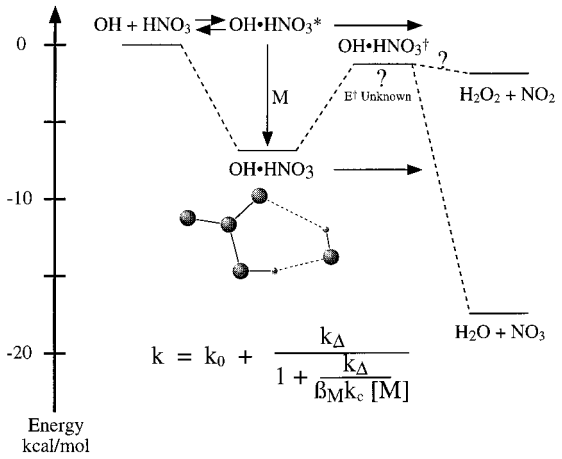

Figure 5. Mechanism for the OH + HNO_3 reaction, including the relative energetics of reactants and products and an estimate of the energy and structure of a possible intermediate.

(anhydrous HNO_3 samples) and present (aqueous HNO_3) are the same. Thus small amounts of water vapor (in comparison to the number density of the buffer gas) must have no effect on k_1.

B. Reaction Mechanism and Validity of the Fit Function. Several authors[8,9,11,15] have suggested possible reaction mechanisms that could give rise to the observed pressure and temperature dependence of k_1. Our purpose in discussing the mechanism here is to present a physical basis for the fit function that we have used in analyzing our data. A more detailed discussion of the reaction mechanism, including rate constants for reactions of isotopically labeled compounds and ab initio calculations of possible reaction intermediates and pathways, will appear in a future publication.[22]

Figure 5 outlines one possible reaction mechanism that is consistent with the observed pressure and temperature dependence. The first step is the formation of an excited complex, $OH{\cdot}HNO_3$*. The excited complex may redissociate, react directly to form products, or collisionally stabilize to form a more stable intermediate, $OH{\cdot}HNO_3$, which also decomposes to form products. Direct reaction of $OH{\cdot}HNO_3$* to products, which is essentially the same as direct H-atom abstraction by OH, likely proceeds over at least a small barrier and should, therefore, display a positive temperature dependence and no pressure dependence. Complex formation, on the other hand, is more likely to behave as an association reaction, with a negative temperature dependence and a positive pressure dependence. The observed k_1 suggest that the latter mechanism increases in importance as the temperature decreases below room temperature. The temperature and pressure dependences above 298 K suggest increasing participation by the "direct" mechanism. The only available high-temperature study[23] reports a rate constant at very high temperature, 1000−1100 K, of $(1.6 \pm 0.3) \times 10^{-13}$ cm^3 molecule^{-1} s^{-1}. The approximately 60% increase in k_1 from 350 to 1000 K suggests a weak positive temperature dependence.

Lamb et al.[11] have shown that the above reaction scheme gives rise to the following form for k_1.

$$k_1 = k_0 + \frac{k_\Delta}{1 + \frac{k_\Delta}{\beta_M k_c [M]}} \qquad (5)$$

Here k_0 is the low-pressure limiting bimolecular rate constant arising from the direct reaction, k_Δ is the difference between the low-pressure and high-pressure limiting rate constants ($k_\Delta = k_\infty - k_0$), k_c is a termolecular rate constant for the complex stabilization step and β_M is the relative stabilization efficiency for each bath gas. We fit our data by assuming that the temperature dependence for each of the three rate constants follows an Arrhenius form.

TABLE 2: Fit Parameters for the Expression $k_1 = k_0 + k_\Delta/[1 + k_\Delta/\beta_M k_c[M]]$[a]

$k_0 = (2.41 \times 10^{-14}) \exp(460/T)$ cm^3 molecule^{-1} s^{-1}
$k_\Delta = (2.69 \times 10^{-17}) \exp(2199/T)$ cm^3 molecule^{-1} s^{-1}
$k_c = (6.51 \times 10^{-34}) \exp(1335/T)$ cm^6 molecule^{-1} s^{-1}
$\beta(He) = 0.38$
$\beta(N_2) = \beta(O_2) = \beta(air) = 1.0$
$\beta(SF_6) = 1.35$

[a] All temperatures in Kelvin.

$$k_i = A_i \exp(-E_i/RT) \qquad i = 0, \Delta, c \qquad (6)$$

We assume this form for even the termolecular rate constant for convenience, even though it is not necessarily theoretically justified. We simultaneously fit all of our data in He, N_2, and SF_6, as well as the data of Stachnik et al.,[15] Margitan and Watson,[9] and Devolder et al.,[12] to arrive at a global fit. The previous section describes the reasons for including the data from only these three literature studies. The fit constrains the high-pressure ($k_\infty = k_0 + k_\Delta$) and low-pressure ($k_0$) limiting bimolecular rate constants in eq 5 to be the same for each of the three bath gases (N_2, He, and SF_6) and gives each a different relative efficiency, β_M, with $\beta(N_2)$ arbitrarily assigned to unity. For the sake of simplicity, we have not considered a temperature dependence for the β values. Table 2 lists the fit parameters.

Figure 5 also shows the relative energetics of the possible reactive complex and the reaction products. The most likely structure for the complex is a doubly hydrogen bonded, six membered ring,[9,15] although other possibilities exist.[11] Nitric acid binds with H_2O in an analogous fashion, and ab initio calculations of the $H_2O{\cdot}HNO_3$ complex find the binding energy to be approximately 7 kcal/mol.[24] Figure 5 shows such an intermediate and assumes similar energetics for $OH{\cdot}HNO_3$. The energetics of the two possible exothermic reaction product channels, reactions 1a and 1b above, also appear in Figure 5. Although there is no direct evidence for the production of $H_2O_2 + NO_2$ from reaction 1, it cannot be ruled out as a minor pathway. One previous study to address this question[7] detected the NO_3 product by absorption at 662 nm and found its yield to be 0.98 ± 0.20 at 298 K and 1.17 ± 0.19 at 251 K (both at approximately 50 Torr pressure). The measurement relied on a recommendation for the 662 nm NO_3 absorption cross section ($\sigma = 1.70 \times 10^{-17}$ cm^2 [25−27]) that has since been revised. A reanalysis of the data with the currently recommended cross section ($\sigma = 2.23 \times 10^{-17}$ cm^2 [28]) gives yields for NO_3 production of 0.75 at 298 and 0.89 at 251 K. Nelson et al.[29] and Jourdain et al.[6] also reported near unit yields of NO_3 at 298 K. Experiments are currently underway in this laboratory to reassess the product yields for reaction 1.

C. Atmospheric Implications. Figure 6 is a comparison of our measured k_1 and fits in N_2 between 200 and 325 K to the current NASA recommendation.[1] The solid lines are the global fit for N_2 as a buffer gas (see Table 2), and the dashed lines are the NASA recommendations at the same temperatures. As described in section A, the recommendation is close to the data near room temperature, but significantly underestimates the pressure dependence at low temperature. At 200 K and 100 Torr, for example, the new fit is a factor of 2 larger than the

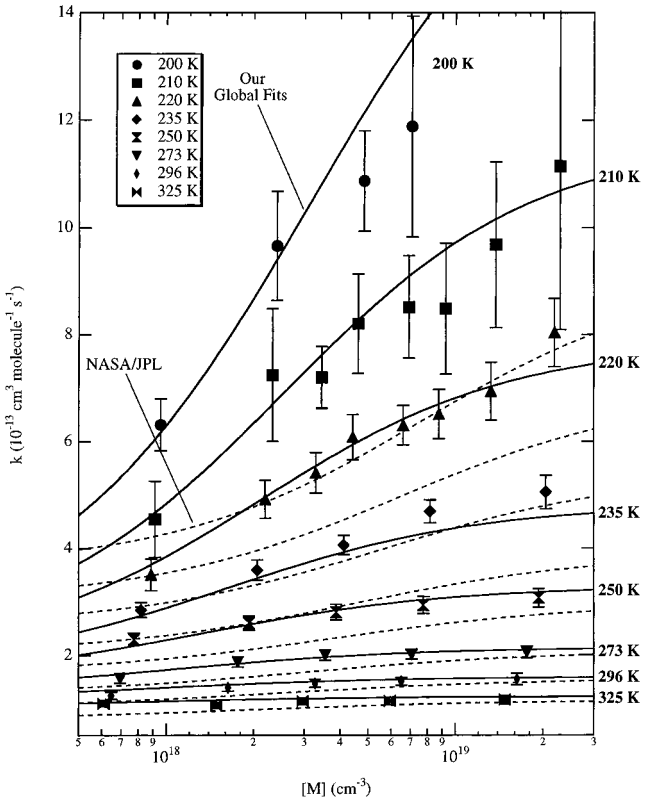

Figure 6. Pressure dependences for k_1 in N_2 between 200 and 325 K. The discrete points are measurements from this work, as the legend shows. The solid curves are the global fits to eq 5 relevant for N_2, and the dashed curves are the current NASA/JPL recommendation for atmospheric modeling.

recommendation. Because of the similarity of k_1 in O_2 and N_2 buffer gases, the N_2 fit is appropriate for the atmosphere.

The difference between new k_1 measurements and the NASA/JPL recommendation has a significant impact on the understanding of the balance between NO_x and NO_y (the sum of all odd nitrogen species) in the lower stratosphere. Since NO_x is the component directly involved in O_3 chemistry, the ratio, NO_x/NO_y, is important for quantifying ozone in the lower stratosphere. In addition to the results presented here, we have recently measured the rate constant for reaction 2, the addition of OH to NO_2 to form HNO_3, and found it to be 15−30% smaller than the NASA recommendation at lower stratospheric temperatures and pressures.[30] The smaller rate constant for reaction 2, together with the much larger k_1, significantly shifts the calculated NO_x/NO_y ratio in favor of NO_x in atmospheric models. The inclusion of the new rate constants in the analysis of data from recent atmospheric measurement campaigns has improved the agreement between photochemical models and observations.[31] An increase in the NO_x/NO_y ratio increases the calculated importance of NO_x-catalyzed ozone destruction relative to other ozone loss mechanisms. The effect on calculated ozone abundance is further increased by recent measurements from this laboratory on the reaction of O atoms with NO_2,[32] the rate-limiting step in the key NO_x-catalyzed O_3 destruction cycle, showing this rate constant to be 20−30% larger in the stratosphere than currently assumed.[1] One important consequence of the new measurements will be to increase the projected impact of stratospheric NO_x pollution from sources such as aircraft engines.

Acknowledgment. We thank Roberto Bianco for many useful discussions about the mechanism for reaction 1. This work was funded in part by NOAA's Climate and Global Change Research Program. S.S.B. held an NOAA/NRC postdoctoral research fellowship during this work.

References and Notes

(1) DeMore, W. B.; Sander, S. P.; Golden, D. M.; Hampson, R. F.; Kurylo, M. J.; Howard, C. J.; Ravishankara, A. R.; Kolb, C. E.; Molina, M. J. Chemical Kinetics and Photochemical Data for Use in Stratospheric Modeling. JPL Publication 97-4; JPL: Pasadena, CA, 1997.

(2) Wine, P. H.; Ravishankara, A. R.; Kruetter, N. M.; Shah, R. C.; Nicovich, J. M.; Thompson, R. L.; Wuebbles. *J. Geophys. Res.* **1981**, *86*, 1105.

(3) Smith, I. W. M.; Zellner, R. *Int. J. Chem. Kinet.* 1975, Symp. 1, 341.

(4) Margitan, J. J.; Kaufman, F.; Anderson, J. G. *Int. J. Chem. Kinet.* 1975, Symp. 1, 281.

(5) Kurylo, M. J.; Cornett, K. D.; Murphy, J. L. *J. Geophys. Res.* **1982**, *87*, 3081.

(6) Jourdain, J. L.; Poulet, G.; Le Bras, G. *J. Chem. Phys.* **1982**, *76*, 5827.

(7) Ravishankara, A. R.; Eisele, F. L.; Wine, P. H. *J. Phys. Chem.* **1982**, *86*, 1854.

(8) Marinelli, W. J.; Johnston, H. S. *J. Chem. Phys.* **1982**, *77*, 1225.

(9) Margitan, J. J.; Watson, R. T. *J. Phys. Chem.* **1982**, *86*, 3819.

(10) Smith, C. A.; Molina, L. T.; Lamb, J. J.; Molina, M. J. *Int. J. Chem. Kinet.* **1984**, *16*, 41.

(11) Lamb, J. J.; Mozurkewich, M.; Benson, S. W. *J. Phys. Chem.* **1984**, *88*, 6441.

(12) Devolder, P.; Carlier, M.; Pauwels, J. F.; Sochet, L. R. *Chem. Phys. Lett.* **1984**, *111*, 94.

(13) Jolly, G. S.; Paraskevopoulos, G.; Singelton, D. L. *Chem. Phys. Lett.* **1985**, *117*, 132.

(14) Connell, P. S.; Howard, C. J. *Int. J. Chem. Kinet.* **1985**, *17*, 17.

(15) Stachnik, R. A.; Molina, L. T.; Molina, M. J. *J. Phys. Chem.* **1985**, *90*, 2777.

(16) Vaghjiani, G. L.; Ravishankara, A. R. *J. Phys. Chem.* **1989**, *93*, 1948.

(17) Burkholder, J. B.; Talukdar, R. K.; Ravishankara, A. R.; Soloman, S. *J. Geophys. Res.* **1993**, *98*, 22, 937.

(18) Dieke, G. H.; Crosswhite, H. M. *J. Quantum Spectrosc. Radiat. Transfer.* **1962**, *2*, 97.

(19) Biaume, F. *J. Photochem.* **1973**/**1974**, *2*, 139.

(20) Johnston, H. S.; Miller, C. E.; Oh, B. Y.; Patten, K. O., Jr.; Sisk, W. N. *J. Phys. Chem.* **1993**, *97*, 9890.

(21) Crowley, J. N.; Burrows, J. P.; Moortgat, G. K.; Poulet, G.; Le Bras, G. *Int. J. Chem. Kinet.* **1993**, *25*, 795.

(22) Brown, S. S.; Talukdar, R. K.; Bianco, R.; Ravishankara, A. R. Manuscript in preparation.

(23) Troe, J. *Ber. Bunsen-Ges. Phys. Chem.* **1974**, *78*, 74.

(24) Tao, F.-M.; Higgins, K.; Klemperer, W.; Nelson, D. D. *Geophys. Res. Lett.* **1996**, *23*, 1797.

(25) Graham, R. A.; Johnston, H. S. *J. Phys. Chem.* **1978**, *82*, 254.

(26) Magnotta, F.; Johnston, H. S. *Geophys. Res. Lett.* **1980**, *7*, 769.

(27) Mitchell, D. N.; Wayne, R. P.; Allen, P. J.; Harrison, R. P.; Twin, R. J. *J. Chem. Soc., Faraday Trans. 2* **1980**, *76*, 785.

(28) Yokelson, R. J.; Burkholder, J. B.; Fox, R. W.; Talukdar, R. K.; Ravishankara, A. R. *J. Phys. Chem.* **1994**, *98*, 13144.

(29) Nelson, H. H.; Marinelli, J.; Johnston, H. S. *Chem. Phys. Lett.* **1981**, *78*, 495.

(30) Brown, S. S.; Talukdar, R. K.; Ravishankara, A. R. *Chem. Phys. Lett.* **1999**, *299*, 277.

(31) Gao, R.-S.; Fahey, D. W.; DelNegro, L. A.; Donnelly, S. G.; Keim, E. R.; Neuman, J. A.; Teverovski, L.; Wennberg, P. O.; Hanisco, T. F.; Lazendorf, E. J.; Proffitt, M. H.; Margitan, J.; Wilson, J. C.; Elkins, J. W.; Stimpfle, R. M.; Cohen, R. C.; McElroy, C. T.; Bui, T. P.; Salawitch, R. J.; Brown, S. S.; Ravishankara, A. R.; Portman, R. W.; Ko, M. K. W.; Weisenstein, D. K.; Newman, P. A. *Geophys. Res. Lett.*, in press.

(32) Gierzack, T.; Burkholder, J. B.; Ravishankara, A. R. *J. Phys. Chem. A* **1999**, *103*, 877.